

CIGS nanostructure: preparation and study using liquid phase method

P. Jakhmola^{1,2} · P. K. Jha^{1,2} · S. P. Bhatnagar^{1,2}

Received: 27 March 2015 / Accepted: 30 May 2015 / Published online: 10 July 2015
© The Author(s) 2015. This article is published with open access at Springerlink.com

Abstract Present study is motivated by interesting attainment obtained for copper indium gallium diselenide compound as a light absorbing material for thin-film solar cell. Formation of copper indium gallium diselenide nanostructures via solvothermal method using starting precursors of copper, indium, gallium salts, and selenium powder is represented. Preparation is done by varying x (0.1 and 0.3) in $\text{CuIn}_{1-x}\text{Ga}_x\text{Se}_2$ compound at a constant temperature and using ethanolamine as a solvent. Characterization of nanostructures is done using powder X-ray diffraction, scanning electron microscopy, dynamic light scattering, Fourier transform infrared spectroscopy, and UV–Vis spectroscopy. It is found that grown chalcopyrite structure at different x , possess agglomeration in nanostructures. Results indicate that presence of 10 % gallium in copper indium gallium diselenide compound leads to the single-phase growth, prepare at the temperature of 190 °C for 19 h.

Keywords Copper indium gallium diselenide · Characterization · Nanostructures

Introduction

Among the group I–III–VI₂ semiconductor material, copper indium gallium (di) selenide is reported the highest efficiency of 20 % as a solar cell device (Jackson et al.

2011). Numerous processes have been reported by many investigators for the synthesis of copper indium gallium diselenide (CIGS) nanostructures like mechanochemical (Rehani et al. 2013), colloidal route (Tang et al. 2008; Kim et al. 2005), green synthesis (Juhaiman et al. 2010), precipitation (Panthani et al. 2008), micro-wave synthesis (Bensebaa et al. 2010), mechanical alloying (Vidhya et al. 2011), etc. A very few reports had been perceived by solution-based techniques for the successful synthesis of CIGS nanoparticles in which reaction time, temperature, reagents, solvent, variation of Ga content, and optimal process are used for synthesis of CIGS nanostructures (Caballero et al. 2009; Repins et al. 2008; Bremond et al. 2007). Main approaches to synthesize nanoparticles are categorized in top-down (source material is reduced from bulk size to nanoscale e.g. grinding) and bottom-up (piecing together of tiny systems to give rise grand systems) approaches. Vapor-phase (e.g., pyrolysis) and liquid-phase fabrication (e.g., solvothermal, sol-gel) are sub-categorized form of bottom-up approaches.

In present work, single-phase $\text{Cu}(\text{In}_{1-x}\text{Ga}_x)\text{Se}_2$ nanostructures have been synthesized via solvothermal approach by using ethanolamine as a solvent. To the best of our knowledge, there are very few reports on the synthesis of as-grown particles via mentioned technique. General concept for the liquid-phase fabrication process based on the solvothermal approach to demonstrate that the nanostructure formation is shown in Fig. 1.

Experimental details

Cupric chloride (>99.0 %) and selenium powder (99.5 %) have been purchased from S D fine, whereas Indium (III) chloride (99.99 %) and Gallium (III) chloride (99.99 %)

✉ P. Jakhmola
priya198508@gmail.com

¹ Department of Physics, Maharaja Krishnakumar Sinhji Bhavnagar University, Bhavnagar 364001, India

² Department of Physics, Maharaja Sayajirao University of Baroda, Vadodara 390002, India

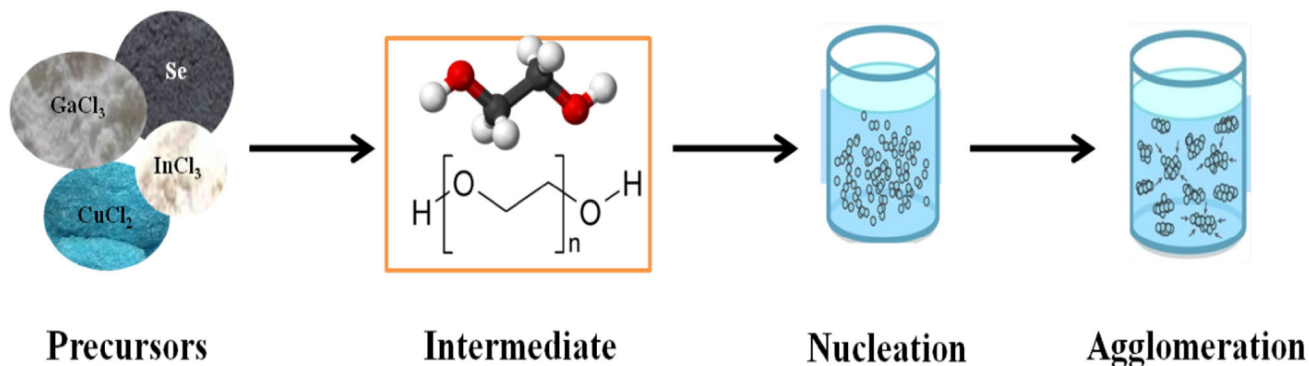
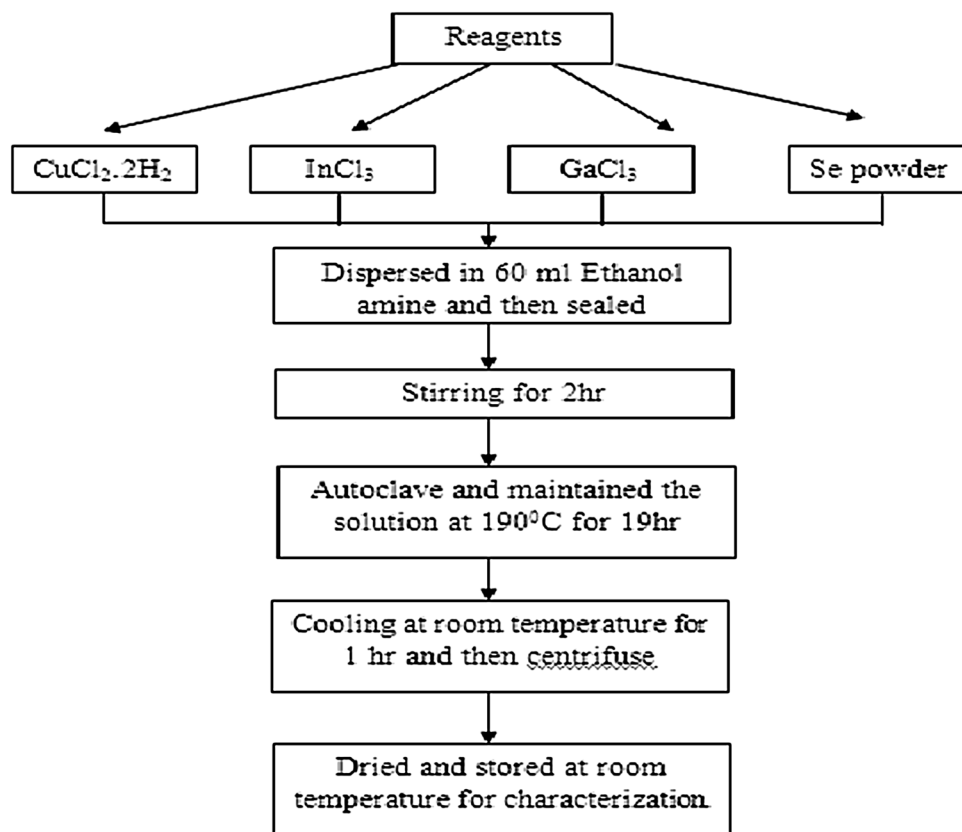


Fig. 1 General concept of the liquid-phase fabrication process based on the solvothermal approach

Fig. 2 The experimental procedure of CIGS nanoparticles growth via solvothermal process



are from Sigma-Aldrich. Ethanolamine is purchased from Merck MSDS. All reagents are used as received without any further purification.

Figure 2 shows the experimental procedure of CIGS nanoparticles growth via solvothermal process. In a systematic experimental procedure, the synthesis of CIGS nanoparticles obtained by varying $x = 0, 0.1,$ and 0.3 in $\text{Cu}(\text{In}_{1-x}\text{Ga}_x)\text{Se}_2$ nanostructure. Salts of dihydrate cupric chloride (0.15 g), Indium (III) chloride ($1 - x$), Gallium (III) chloride (x), and Se (0.300 g) powder were loaded in a beaker containing 60 ml of ethanolamine. The mixture

is magnetic stirred for 2 h at room temperature measured $32\text{ }^\circ\text{C}$, solution is turned into deep black from initial dark blue for both $x = 0.1$ and 0.3 . The solution is autoclave and maintained at a temperature of $190\text{ }^\circ\text{C}$ for 19 h . The reaction is now allowed to cool at room temperature and finally black-colored particles are obtained. Methanol is added to as obtained product and then sonicate for 10 min . Further the solution is centrifuge around 30 min and then rinse with distill water and acetone several times. Final obtained product is dried for further characterization.

As-obtained product is first characterized by powder X-ray diffraction Rigaku miniflex-II using $\text{CuK}\alpha$ with 1.54060 \AA radiations in the 2θ range from 10° to 90° while the voltage and current are held at 40 kV and 30 mA, respectively. Surface morphology is studied by scanning electron microscopy using model LEO 1430 VP. Particle size is determined by dynamic light scattering using Malvern mastersizer 2000. Optical spectra are recorded using ELICO BL-198 in the range of 380–1100 nm and the energy band gap is also evaluated.

Results and discussion

The structural analysis of synthesized CIGS nanostructures has been determined using X-ray diffraction. Figure 3a–c shows diffraction features of chalcopyrite structure of CIS and CIGS nanostructures. We can see that for diffraction pattern of CuInSe_2 and $\text{Cu}(\text{In}_{0.9}\text{Ga}_{0.1})\text{Se}_2$ synthesized at 190°C for 19 h, sharp and intense diffraction peaks are detected at diffraction angle 26.92° , 44.47° , and 52.65° , shows chalcopyrite tetragonal structure by making match with the Joint Committee on Powder Diffraction Standards (JCPDS) card File No. 27-0159 (Alberts 2004). These peaks correspond to the preferred orientation plane of (112), (220/204), and (332/116), respectively. The less intense peaks observed at 71.06° and 81.62° correspond to the planes (332/316) and (424/228), respectively. For $\text{Cu}(\text{In}_{0.9}\text{Ga}_{0.1})\text{Se}_2$ and $\text{Cu}(\text{In}_{0.7}\text{Ga}_{0.3})\text{Se}_2$ compound, the presence of the peaks at (400/008) and (424/228) orientation results that Ga takes partly the place of indium in tetragonal phase and then result in tetragonal CIGS phase. It is clear that single phase is obtained when x is taken 0.1, revealing active participation of gallium in the formation of tetragonal chalcopyrite CIGS structure (see Fig. 3d). However, at $x = 0.3$, we can observe few secondary phases or decrease in the quality of crystallinity and increase of defects in XRD pattern. It reveals that proper ratio of indium and gallium is necessary during synthesis. The FWHM of (112) peak increases with increasing x given in Table 1 and hence decrease in grain size and should be ascribed to the lowest crystalline quality of the sample clearly outlined in Fig. 3c. The microstructure obtained by scanning electron microscopy is shown in Fig. 4a–c labeled as (a) CuInSe_2 (without gallium), (b) $\text{Cu}(\text{In}_{0.9}\text{Ga}_{0.1})\text{Se}_2$, and (c) $\text{Cu}(\text{In}_{0.7}\text{Ga}_{0.3})\text{Se}_2$ nanostructures. We observe a remarkable difference in shape and size in samples without and with Ga. Dependence of gallium content on grain size interprets that the atomic radii of gallium are smaller than indium hence greater amount of gallium results in smaller grain size (Alberts 2004, 2009; Souilah et al. 2009; Zhang et al. 2009). Figure 4b, c shows soft agglomeration, also merging

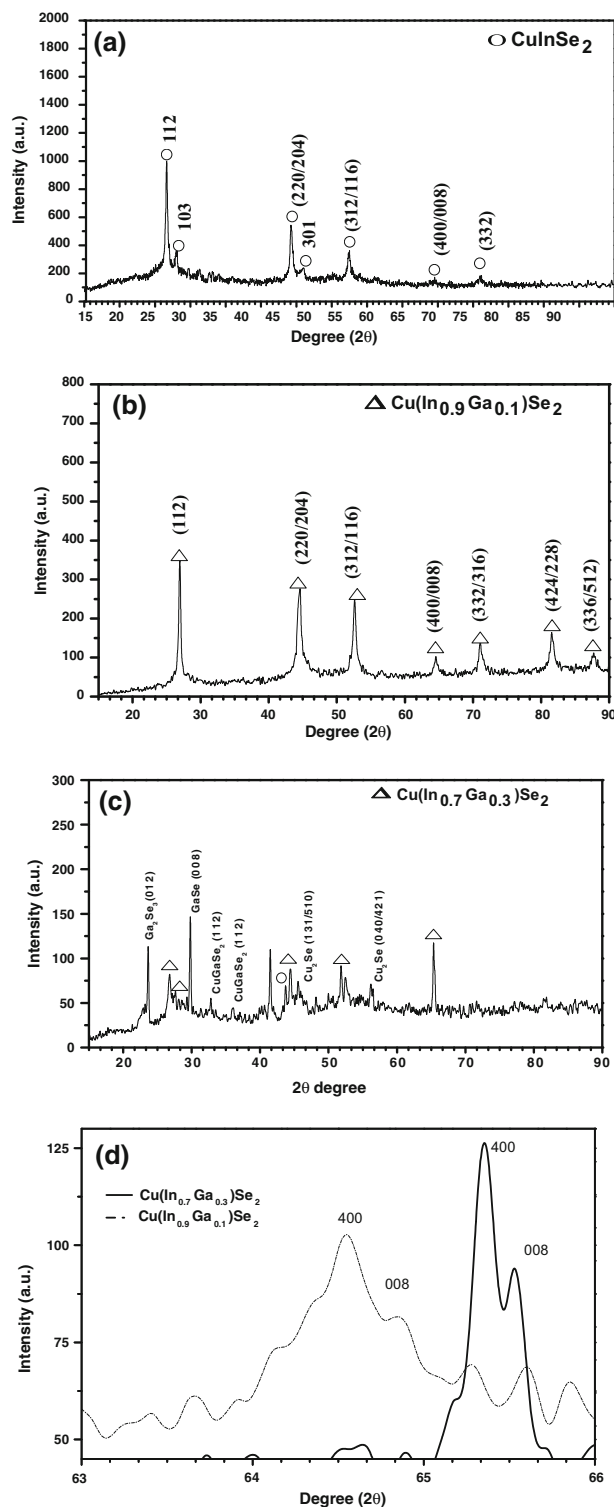
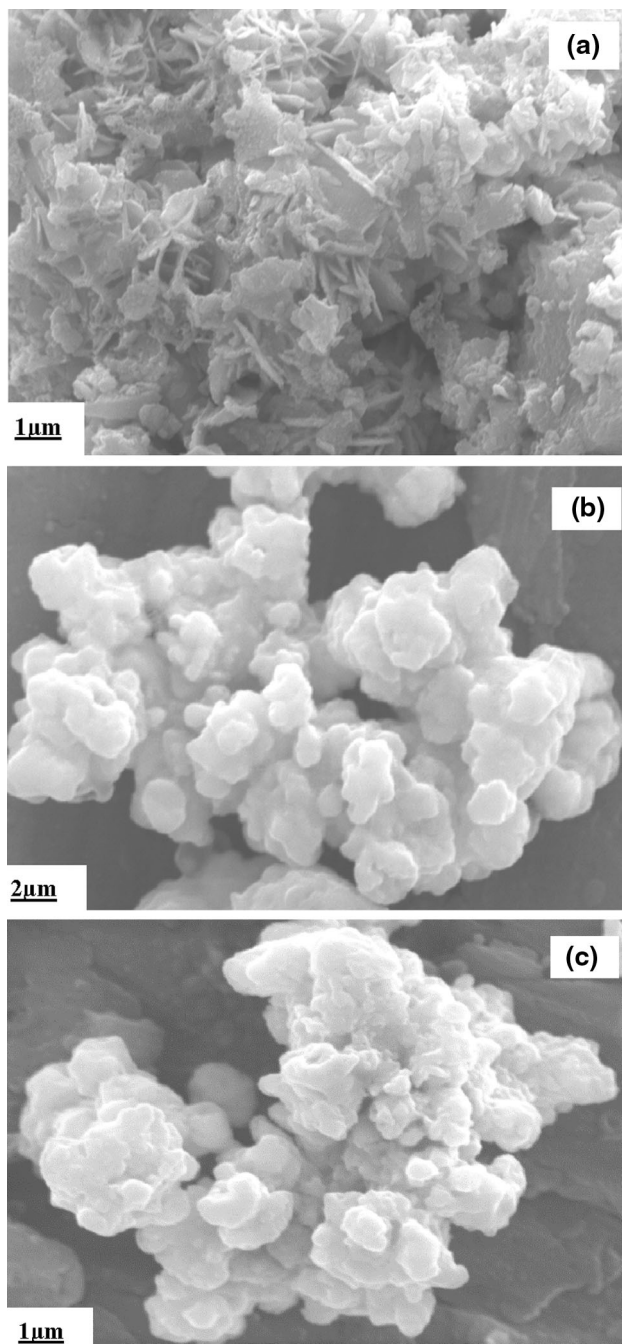
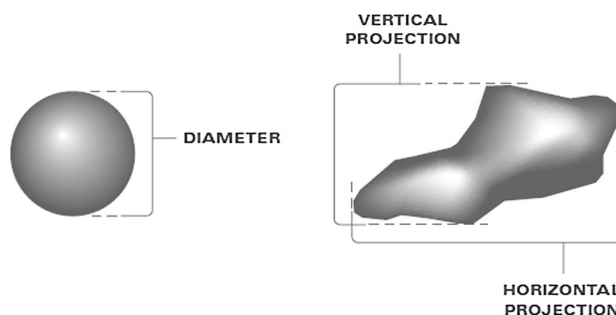


Fig. 3 X-ray diffraction of CuInSe_2 , $\text{Cu}(\text{In}_{0.9}\text{Ga}_{0.1})\text{Se}_2$, and $\text{Cu}(\text{In}_{0.7}\text{Ga}_{0.3})\text{Se}_2$ nanostructures grown via solvothermal approach at 190°C for 19 h

boundaries, non-spherical, and irregular formation of nanoparticles at $x = 0.1$ and 0.3 , respectively. It may interprets that gallium content in the compound may play

Table 1 Comparison of particle size obtained by DLS and XRD

Compound	Particle size D (nm) XRD	Particle size D (nm) DLS	FWHM (112)
CuInSe ₂	123	124	0.2309
CuIn _{0.9} Ga _{0.1} Se ₂	64	65	0.2460
CuIn _{0.7} Ga _{0.3} Se ₂	48	50	0.5904

**Fig. 4** Scanning electron microscopy for **a** CuInSe₂, **b** Cu(In_{0.9}Ga_{0.1})Se₂, and **c** Cu(In_{0.7}Ga_{0.3})Se₂ nanostructure**Fig. 5** Size determination for non-spherical particles can be described using multiple length and width measures (horizontal and vertical projections)

an important role in the growth of nanoparticles in particular direction.

Particle size of as-grown nanostructure is measured by dynamic light scattering (DLS) at room temperature. Size determination by a light scattering device for spherical particle can be described using diameter, because every dimension of spherical particle is identical. Figure 5 shows, in case of non-spherical particles, to provide greater accuracy, that the size evaluation can be done using multiple length and width measures (horizontal and vertical projections). A light-scattering device makes an average for various dimensions, as the particles flow randomly through the light beam, producing a distribution of sizes from the smallest to the largest dimensions.

In our work, before taking DLS measurement, sample is filtered by micro-filter kit of 0.45 μm pore size to remove dust particles. Sonication is also done to remove agglomeration, which effects DLS measurements. To make the measurement, the as-grown product is dispersed in methanol. Before taking particle size measurement, we first evaluate the correlation function. Figure 6a–c shows the size distribution curve of as-grown particles. The average diameters of synthesized nanostructures are evaluated as 124, 65, and 50 nm for CuInSe₂, Cu(In_{0.9}Ga_{0.1})Se₂, and Cu(In_{0.7}Ga_{0.3})Se₂, respectively, which demonstrate that grain size and grain boundaries of CIGS nanostructure decrease with increase in Ga content. It is found that the estimated particle size by XRD and DLS differs; it still interprets agglomeration formation in as-grown nanostructures. Table 1 enlists the comparison of particle size, calculating by XRD and measuring through DLS.

Figure 7 shows the absorption spectra of CIS and CIGS with varying gallium content. The absorption spectra of CIGS are recorded in the range of 380–1100 nm using methanol as reference. The sharp absorption edges at the fundamental absorption region shift toward lower wavelength by increasing gallium content from $x = 0, 0.1,$ and 0.3 . Simultaneously, magnitude of absorption near the fundamental absorption edge decreases because of

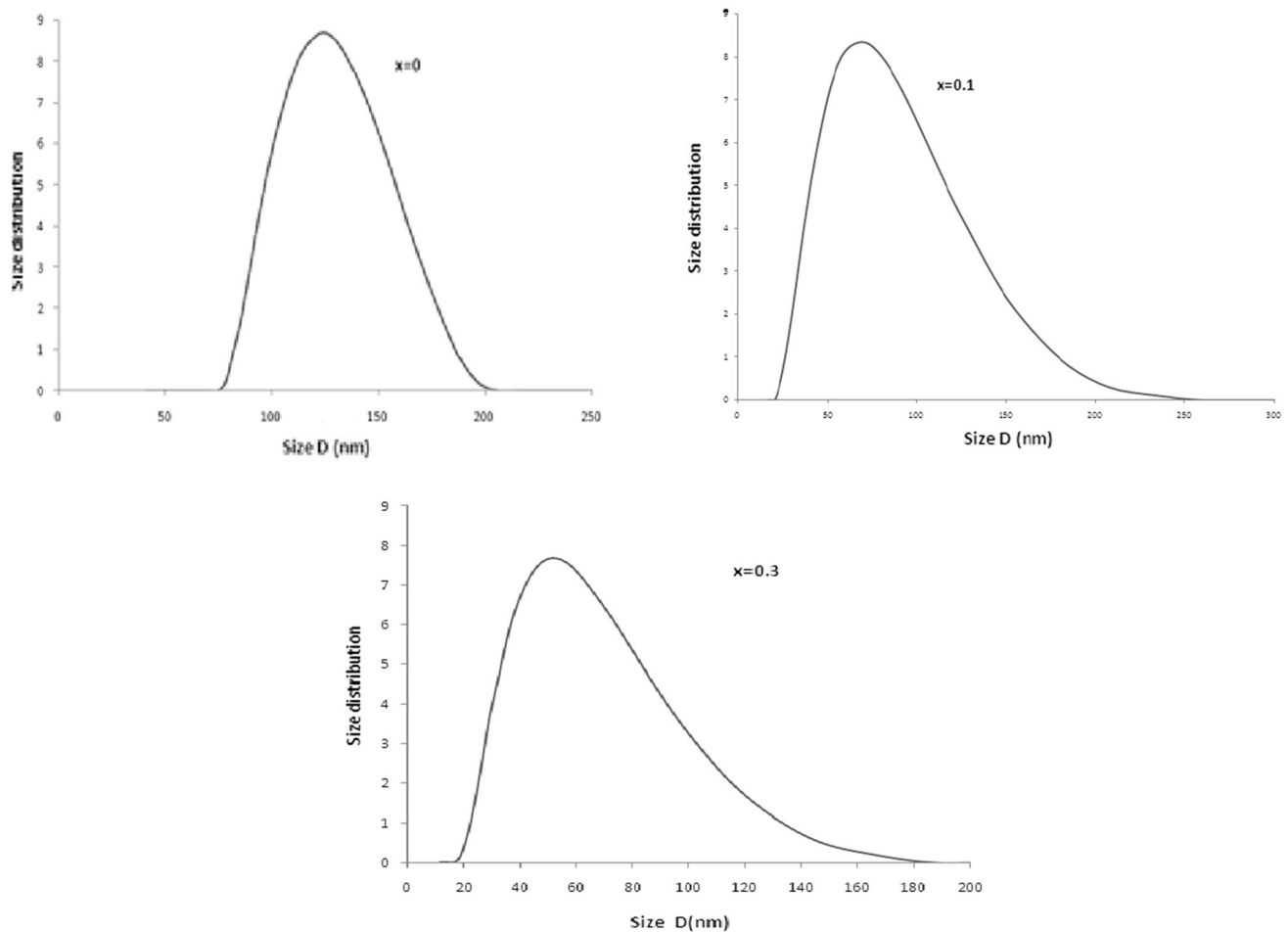


Fig. 6 Size distribution curve of CuInSe_2 ($x = 0$), $\text{Cu}(\text{In}_{0.9}\text{Ga}_{0.1})\text{Se}_2$ ($x = 0.1$) and $\text{Cu}(\text{In}_{0.7}\text{Ga}_{0.3})\text{Se}_2$ ($x = 0.3$) nanostructure

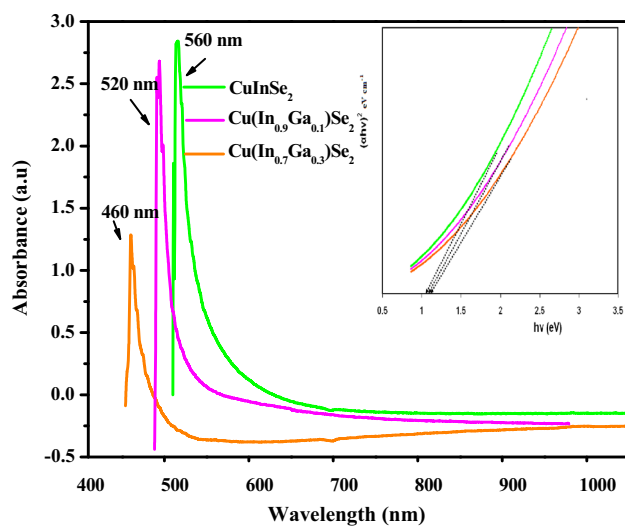


Fig. 7 Absorption spectrum of CuInSe_2 , $\text{Cu}(\text{In}_{0.9}\text{Ga}_{0.1})\text{Se}_2$, and $\text{Cu}(\text{In}_{0.7}\text{Ga}_{0.3})\text{Se}_2$ prepared in ethanolamine

decreasing grain sizes due to an increase of Ga content and more grain boundaries, which scattered incident light. However, large onset of all three nanostructures reveals

wide range of particle size distribution. For $x = 0, 0.1$, and 0.3 , the calculated optical band gaps are 1.02, 1.10, and 1.20 eV, respectively (shown in the inset of Fig. 7). In short, the CIGS samples show bowing in band gaps with variation of Ga composition. The bandgap evaluated of $\text{CuIn}_{1-x}\text{Ga}_x\text{Se}_2$ compound nearly matches with solar spectrum and can be used as an absorber layer in thin-film solar cells.

This technique provides information about the chemical bonding in a material. It is used to identify the elemental constituents of a material. Figure 8 shows the Fourier transform infrared (FTIR) spectra of as prepared single-phase copper indium gallium diselenide (CIGS) nanoparticles. Before FTIR measurement, the sample is milled with KBr to form a fine powder. The spectra range is taken from 400 to 4000 cm^{-1} assign vibration spectra of the compound. Before FTIR analysis, the samples are rinsed with methanol and distill water several times and then dried at $60\text{ }^\circ\text{C}$ for 1 h.

Figure 8 shows the FTIR spectra of single-phase CIS ($x = 0$) and CIGS ($x = 0.1$) compound. From Fig. 8a, the

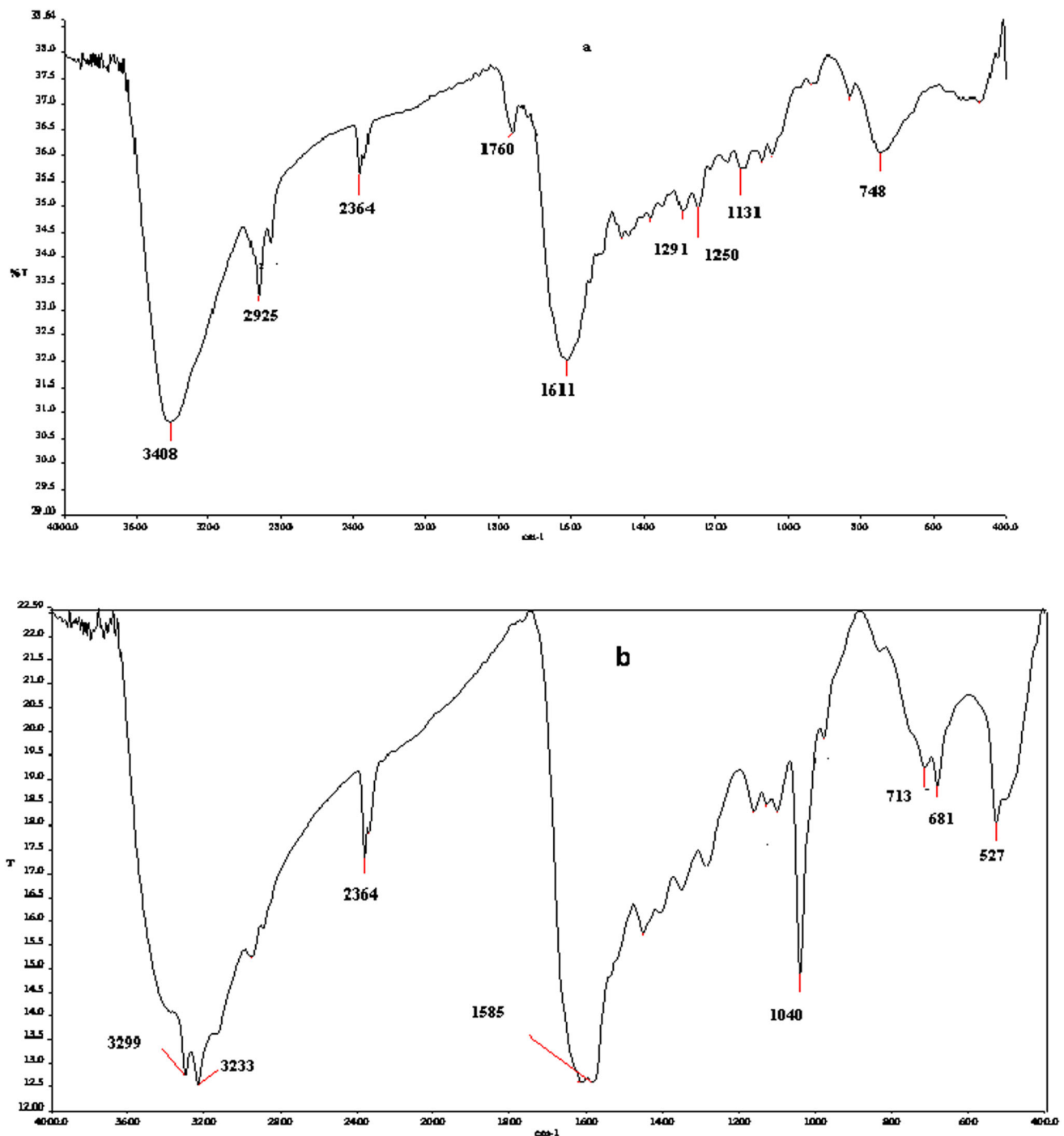


Fig. 8 FTIR spectra of single-phase CIS ($x = 0$) and CIGS ($x = 0.1$) compound

broad peak is observed at 3408 cm^{-1} assigned to -OH stretching intermolecular hydrogen bonds due to the small quantity of H_2O or moisture on the sample. The vibration peak at 2925 cm^{-1} assigns to O-H stretch due to rinsing sample with methanol several times. The weak and sharp peaks at 2364 cm^{-1} assign to C-H stretch confirms formation of $[\text{Cu(en)}]^+$ in the compound. N-H stretching

vibration peak is observed at 1611 cm^{-1} due to preparation of CuInSe_2 in the ethylenediamine. Broad peak observed at 748 cm^{-1} , recognized as C-H bond (disubstituted), reveals chelate formation in CIS compound. As shown in Fig. 8b, the two sharp peaks at 3299 and 3233 cm^{-1} assigned N-H stretch due to ethanolamine used for synthesis. Again, vibration broad peak at 1585 cm^{-1} is of N-H bond. Sharp

peak at 1040 cm^{-1} is assigned to C–N stretch that shows formation of chelate complex in ethanolamine. Weak and broad peaks at 713 and 681 cm^{-1} are C–Cl stretch. Again broad peak at 527 cm^{-1} C–Br stretch is due to IR spectra obtained with KBr and NaCl.

Conclusion

Single-phase CIGS nanostructures are successfully synthesized by taking $x = 0.1$ with the starting precursors of dihydrate cupric chloride, Indium (III) chloride, Gallium (III) chloride, and Se powder using ethanolamine as a solvent. The chemical bonding investigated by FTIR of single phase that was obtained at $x = 0$ and 0.1 samples gives the presence of bonds and used to identify the elemental constituent of a material.

Open Access This article is distributed under the terms of the Creative Commons Attribution 4.0 International License (<http://creativecommons.org/licenses/by/4.0/>), which permits unrestricted use, distribution, and reproduction in any medium, provided you give appropriate credit to the original author(s) and the source, provide a link to the Creative Commons license, and indicate if changes were made.

References

- Alberts V (2004) Band gap engineering in polycrystalline $\text{Cu}(\text{In,Ga})(\text{Se,S})_2$ chalcopyrite thin films. *Mater Sci Eng B* 107:139–147
- Alberts V (2009) Band gap optimization in $\text{Cu}(\text{In}_{1-x}\text{Ga}_x)(\text{Se}_{1-y}\text{S}_y)_2$ by controlled Ga and S incorporation during reaction of $\text{Cu}(\text{In,Ga})$ intermetallics in H_2Se and H_2S . *Thin Solid Films* 517:2115–2120
- Bensebaa F, Durand C, Aouadou A, Scoles L, Du X, Wang D, Page YL (2010) A new green synthesis method of CuInS_2 and CuInSe_2 nanoparticles and their integration into thin films. *J Nanopart Res* 12:1248–1252
- Bremeud D, Rudmann D, Kalein M, Ernits K, Bilger G, Dobeli M, Zogg H, Tiwari AN (2007) Flexible $\text{Cu}(\text{In,Ga})\text{Se}_2$ on Al foils and the effects of Al during chemical bath deposition. *Thin Solid Films* 515:5857–5861
- Caballero R, Kaufmann CA, Eisenbarth T, Canclea M, Hesse R, Unold T, Eicke A, Klenk R, Schock HW (2009) The influence of Na on low temperature growth of CIGS thin film solar cells on polyimide substrates. *Thin Solid Films* 517:2187–2190
- Jackson P, Hariskos D, Lotter E, Paetel S, Wuerz R, Menner R (2011) New world record efficiency for $\text{Cu}(\text{In,Ga})\text{Se}_2$ thin-film solar cells beyond 20 %. *Prog Photovol Res Appl* 19:894–897
- Juhaiman LA, Scoles L, Kingston D, Patarachao B, Wang D, Bensebaa F (2010) Green synthesis of tunable $\text{Cu}(\text{In}_{1-x}\text{Ga}_x)\text{Se}_2$ nanoparticles using non organic solvents. *Green Chem* 12:1248–1252
- Kim KH, Chun YG, Yoon KH, Park BO (2005) Synthesis of CuInGaSe_2 nanoparticles by low temperature colloidal route. *J Mech Sci Technol* 19:2085–2090
- Panthani MG, Akhavan V, Goodfellow B, Schmidtke JP, Dunn L, Dodabalapur A, Barbara PF, Gorgel BA (2008) Synthesis of CuInS_2 , CuInSe_2 , and $\text{Cu}(\text{In}_x\text{Ga}_{1-x})\text{Se}_2$ (CIGS) nanocrystal “Inks” for printable photovoltaics. *J Am Chem Soc* 130:16770–16777
- Rehani B, Ray JR, Panchal CJ, Master H, Desai RR, Patel PB (2013) Mechanochemically synthesized CIGS nanocrystalline powder for solar cell applications. *J Nano Electron Phys* 5:02007–02010
- Repins I, Contreras MJ, Romero EB, DeHart C, Scarf J, Perkins CJ, To B, Noufi R, Scharf J (2008) 19.9 % efficient $\text{ZnO}/\text{CdS}/\text{CuInGaSe}_2$ solar cell with 81.2 % fill factor. *Prog Photovol Res Appl* 16:235–239
- Souilah M, Rocquefelte X, Lafond A, Guillot-Deudon C, Morniroli JP, Kessler J (2009) Crystal structure re-investigation in wide band gap CIGSe compounds. *Thin Solid Films* 517:2145–2148
- Tang J, Hinds S, Kelley SO, Sargent EH (2008) Synthesis of colloidal CuGaSe_2 , CuInSe_2 , and $\text{Cu}(\text{InGa})\text{Se}_2$ nanoparticles. *Chem Mater* 22:6906–6910
- Vidhya B, Velumani S, Asomoza R (2011) Effect of milling time and heat treatment on the composition of $\text{CuIn}_{0.75}\text{Ga}_{0.25}\text{Se}_2$ nanoparticle precursors and films. *J Nanopart Res* 13:3033–3042
- Zhang L, He Q, Jiang WL, Liu FF, Li CJ, Sun Y (2009) Effects of substrate temperature on the structural and electrical properties of $\text{Cu}(\text{In,Ga})\text{Se}_2$ thin films. *Sol Energy Mater Solar Cells* 93:114–118